# Characterization of Dry Sliding Behavior of a Si-Mo-Cr Ductile Cast Iron

**Nanak Ram**
Research Scholar
Delhi Technological University
Department of Mechanical Engineering
India

**Vijay Gautam**
Professor
Delhi Technological University
Department of Mechanical Engineering
India

*The prerequisites for a brake disc material include a lower specific wear rate, a high coefficient of friction against brake pad material, lighter weight, and a higher heat dissipation rate. The present research studied the dry sliding wear behavior of as-cast Si-Mo-Cr ductile cast iron (DCI). A series of pin-on-disc wear tests are conducted using Taguchi L16 array for the optimum combination of load, sliding velocity, and temperature on a rotary tribometer setup at controlled temperatures ranging from 30°C to 240°C. The analysis of variance, first-order regression analysis, and confirmation tests are done to validate the results obtained for the material's wear properties. SEM and EdX analysis of wear surfaces is also done. It founds that the sliding velocity has a more significant influence on the specific wear rate. In contrast, the applied load is the key influencing parameter for a higher value of the coefficient of friction.*

***Keywords:*** *Si-Mo-Cr DCI, pin-on-disc, specific wear rate, coefficient of friction, Taguchi $L_{16}$ array.*

## 1. INTRODUCTION

Ductile cast iron alloyed with silicon, molybdenum, and chromium (Si-Mo-Cr DCI) has emerged as a potential candidate for application in components for automotive, earth movers, special purpose machinery, and defense equipment [1]. This material offers high tensile strength, toughness, thermal stability, high hardness, high wear resistance, and good heat dissipation properties to meet the requirement of engineers and researchers for various applications at low production costs [2]. According to Delprete and Sesana, Si-Mo-Cr ductile cast iron exhibits strong monotonic qualities at low temperatures. However, it becomes fragile during fatigue tests due to the high silicon content in the alloy [3]. The application of DCI for manufacturing gears, crankshafts, brake discs, etc., where enhanced wear resistance at different temperatures is needed, has drawn the special attention of engineers [4]. The study of the wear behavior of a DCI is a complex phenomenon due to several variables, including constituents of material, surface properties of the component, temperature range, sliding method: translatory or rotary, sliding velocity: high or low, sliding type: dry or wet and sliding pressure [5-7]. The surfaces of the casted components include a variety of defects and distortions, which results in a strong influence on the wear properties of the material [6]. The rise in temperature due to rubbing the contacting surfaces during sliding also contributes to a higher specific wear rate ($k$) which may lead to thermal softening and possible melting of the surface layer of the material [8-9].

Stachowiak and Batchelor stated that the behavior of contacting surfaces during sliding contact is quite different from that of static contact due to the fewer contact surface areas in sliding contact compared to static contact [8]. In dry sliding, a few of the surface particles of the contact surfaces may jump out from their lattice structure under the combined effect of pressure, sliding velocity, and temperature and move along the motion between contact surfaces, termed wear particles. The frictional interaction appears to be controlled by mec–hanical interlocking between such wear lumps on oppo–site surfaces. Mardaras et al. created an innovative tech–nique to deposit layers of chromium carbide, ledeburite, and pearlite on as-cast specimens of DCI to improve the wear resistance and hardness of the surface layer [10].

Shafiee et al. have studied the microstructural effects on the wear behavior of DCI and compared the wear properties of Cr-Mo steel with DCI [1]. Cardoso et al. have compared the austempered DCI and white cast iron in abrasive wear resistance and founds better wear resistance of austempered DCI as compared to white cast iron due to the presence of martensite in the matrix [11]. Zou et al. studied the effect of chromium addition to nodular cast iron [12]. It was concluded that chro–mium addition to nodular cast iron increases the bainite structure in the matrix. Rebasa et al. conducted an experimental study of the effect of varying nodule count in DCI on abrasive wear, and rolling contact fatigue wear [13]. The increase in nodule count resulted in a higher abrasive wear rate. Weiß et al. conducted experimental studies on the effect of silicon content on the mechanical properties of DCI [14]. It was concluded that a silicon content beyond 4.3% reduces the strength and ductility of DCI. Scandian et al. studied the effect of Mo and Cr content in the sliding wear of high chromium white cast iron and concluded that the wear properties are highly influenced by the matrix microstructure instead of the carbide volume fraction and the macroscopic hardness of the material [15].

Received: September 2022, Accepted: December 2022
Correspondence to: Nanak Ram, Delhi Technological University, Shahbad Daulatpur, Main Bawana Road, Delhi 110042, India.
E-mail: nanakram_phd2k15@dtu.ac.in
**doi: 10.5937/fme2301048R**

Many researchers have applied statistical techniques to quantify the effects of various parameters' effects on sliding wear.

Selvaraj et al. optimized the design parameters for a radial tip centrifugal blower using statistical analysis [16]. Prasad studied the sliding wear response of the cast iron at different wear-affecting parameters like applied load, sliding speed, and test environments to understand the wear mechanism of the material [17-18]. It was observed that as the temperature increases with the increase in speed and load while the frictional coef–ficient decreases, the wear loss increases significantly.

Sahin and Durak developed a numerical model to study the wear resistance of DCI and observed that sliding distance was the main factor responsible for abrasive wear using the design of experiments and ANOVA techniques [19]. Kuti et al. have found the tribological analysis of used engine oil to be one of the cost-effective failure analyses of engine components [20]. Kshirsagar and Khairnar observed similar trends for the coefficient of friction in both experimental and analytical approaches [21].

The course of wear patterns of a similar kind was observed by Chernets et al. during the study of spur gear engagement-disengagement [22].

The study of the dry sliding wear behavior of Si-Mo-Cr DCI against the molded brake friction pad has not been reported or researched so far. Therefore, in the pre–sent study, the sliding wear properties, viz., specific wear rate and coefficient of friction for the specimens of Si-Mo-Cr DCI in dry sliding conditions against the molded brake friction pad, are studied using a series of pin-on-disc experiments. The discs for the wear tests are made from the as-cast plates of Si-Mo-Cr DCI, and the pins are made from the brake friction pad material used exten–sively for automotive braking applications. Taguchi L16 array technique [23] is used to optimize the parameters of the pin-on-disc test at different temperatures.

## 2. EXPERIMENTAL PROCEDURE

### 2.1 Material selection

In the present work, as-cast Si-Mo-Cr DCI is selected to study wear properties specific wear rate (*k)*and coef–ficient of friction (*μ)* only. The required material is pre–pared in the metal casting laboratory in DTU by con–trolled melting of pig iron with Ferro-Mo, Ferro-Cr, and Ferro-Si using a charge calculation basis in a 30kW in–duction furnace of 10kg capacity followed by Mg treat–ment in a ladle [24]. Table 1 shows the as-cast samples' representative chemical compositions (in %wt.), and Table 2 summarizes the microstructural details and mechanical properties. C and Si content in the matrix improves the fluidity of the cast material. Adding Mo and Cr stabilizes the pearlitic matrix and acts as a strong carbide former. The controlled addition of Mo and Cr to Si-Mo-Cr DCI improves the mechanical properties, such as tensile strength and hardness, which further enhances the wear properties of the developed material.

**Table 1. Chemical composition of Si-Mo-Cr DCI in %wt**

| C | Si | Mo | Cr | Cu | Mg | Fe |
|---|---|---|---|---|---|---|
| 3.5 | 3.2 | 0.7 | 0.4 | 0.5 | 0.1 | Rest |

**Table 2. Microstructural and mechanical properties of Si-Mo-Cr DCI**

| Microstructural properties | | | | | Mechanical properties | |
|---|---|---|---|---|---|---|
| Nodularity range (%) | Equivalent nodule diameter (μm) | Nodule count (per $mm^2$) | Ferrite (%) | Pearlite (%) | Tensile strength (MPa) | Microhardness (HV0.5) |
| 80-90 | 73 | 117 | 46 | 54 | 535±23 | 298± 10.67 |

### 2.2 Specimen (pin and disc) preparation

The assembly of a small pin made of brake pad material and a pin holder to hold the pin firmly is considered a pin throughout this study. The pin holders, 40 mm in length and 12mm in outer diameter, are made from mild steel. A circular slot of 10 mm diameter and 5mm depth is drilled on one end of each pin holder to hold the pin. The friction pad material of the brake disc is cut to the pin size with the help of an abrasive diamond cutter, and its outer surface is turned into the required shape of the slot provided on the pin holder end, as shown in Figure 1. The pin is fixed firmly in the pin holder pocket with a strong adhesive(Epoxy Bonding Compound). A total of 16 numbers of pins are fabricated for the pin-on-disc experiments. The chemical composition of the brake friction pad is summarized in Table 3. The disc of the required size is first modeled in design software, as shown in Figure 1 (a).

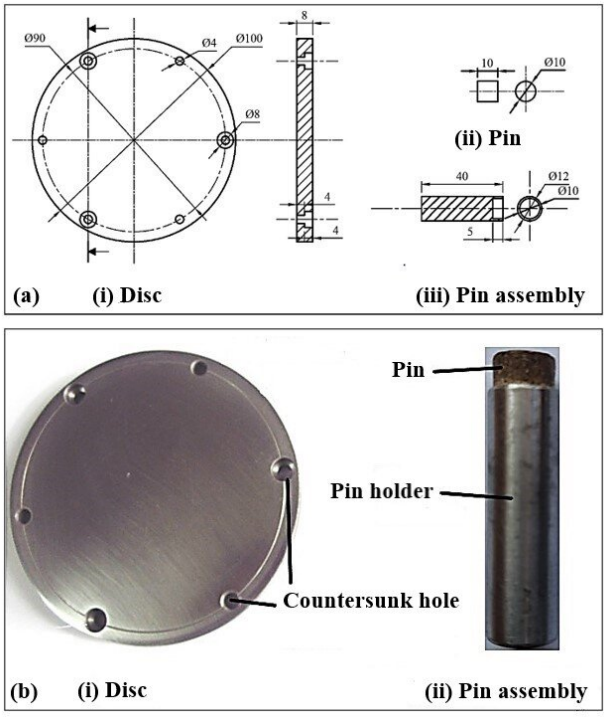


**Figure1. (a) Drawing of disc, pin, and pin holder in mm, (b) Disc and pin assembly specimens**

**Table 3. Chemical composition of friction pad in %wt**

| Si | P | S | Ti | V | Mn | Fe | Cu | Zn | Zr | Sb | C | Al |
|---|---|---|---|---|---|---|---|---|---|---|---|---|
| 7.6 | 4.5 | 5.3 | 27 | 4.3 | 0.4 | 7.4 | 15 | 0.2 | 19 | 3.3 | 0.1 | 5.9 |

The disc for the wear test apparatus is prepared from as-cast plates of Si-Mo-Cr DCI in the required sizes of Ø100 mm x 8 mm by turning operations followed by standard surface finishing operations. Six equidistantly spaced holes of Ø4 mm diameter are drilled at a pitch circle diameter of Ø 90 mm. Also, for securing the disc on the tribometer disc holder with screws, three equidistant 4mm deep countersinking holes of 8 mm diameter are on each side of the disc.

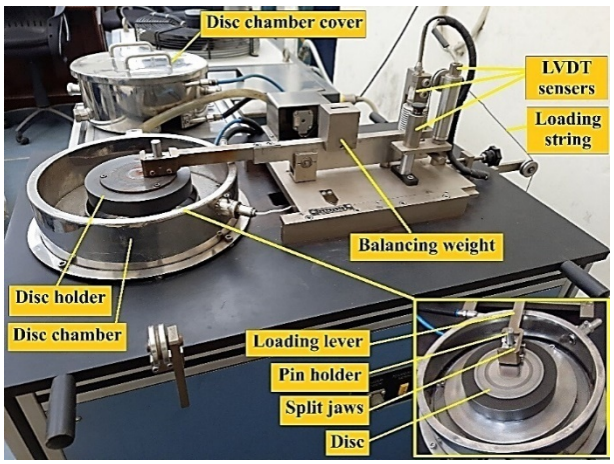


**Figure 2. Experimental setup showing temperature-controlled rotary tribometer**

The dry sliding wear experiments are conducted as per ASTM standard G99-17 on a temperature-controlled rotary tribometer setup (Make: Ducom, Model: TR-20L-PHM800-DHM850) with a complete data acquisition system shown in Figure 2. For conducting the experiments, both surfaces of the disc may be used. Therefore, a total number of 8 discs are prepared for the experimental studies. The experiments will be conducted for four levels comprising different combinations of wear parameters (speed, temperature, and load), as shown in Table 4. Each level value of wear parameters is taken deliberately double the previous one.

**Table 4. Wear test parameters and their levels**

| Sr. no. | Wear test parameters | Levels | | | |
|---|---|---|---|---|---|
| | | 1 | 2 | 3 | 4 |
| 1 | Load, F (N) | 20 | 40 | 80 | 160 |
| 2 | Sliding velocity, v (m/s) | 1.1 | 2.2 | 4.4 | 8.8 |
| 3 | Temperature, T (°C) | 30 | 60 | 120 | 240 |

### 2.3 Wear test

The sliding distance of 3000m is selected for each wear experiment. The disc and pin are cleaned using acetone to remove dirt, grease, and debris. The wear discs are marked to be identified easily for the post-experiment procedures. The formal trial run-in sliding wear of 2-3 minutes is done before the start of the actual test to remove unevenness/debris on the surface of the disc and the pin. After the initial trial run-in, disc and pin surfaces are cleaned again with acetone and weighed separately on a digital scale (least count 0.1 mg). The pin is fixed correctly in the tribometer's pin holder jaws, and the desired track radius is adjusted as the pre–requisite of the experiments. The weight is placed into the load hanger and fed its values in the data acquisition system of the tribometer. The sensors (for friction force measurement and the coefficient of friction mea–surement) are adjusted to zero values. The initial values of friction force, wear, and coefficient of friction value reset to zero in the data acquisition system. The requisite parameters, such as load, sliding velocity, sliding distance, temperature, and sliding track radius, are fed in the data acquisition of the tribometer.

The wear tests are performed only after attaining the requisite temperature in the disc chamber of the tribometer. After each test, the disc and the pin surfaces are cleaned using acetone to remove the wear debris from the surface before the final weight measurement. The variation in parameters like frictional force, coef–ficient of friction, wear, and temperature is recorded continuously on the screen. The recorded data for each wear test is further processed and analyzed using MINITAB statistical software.

### 2.4 Microstructural analysis of wear surface

SEM and EdX analysis are performed on the wear surface of the tested disc specimens using a Zeiss EVO 50 microscope with an attachment of Bruker EdX (Quantax 200). The tested samples are cut into the size of 20mm X 10mm for conducting microstructural ana–lysis. These specimens are cleaned in the acetone solu–tion and dried to ensure all the surfaces are free from moisture, dust, loose wear debris, grease, and oil traces. These cleaned and dried specimens are placed on a pallet (Ø50 mm) inside the vacuum chamber designed to have a vacuum of $10^{-4}$ mbar. The microscopic exa–mination is performed at different analytical working distances and magnification levels. The EdX analysis is done on the disc specimens to examine the embedded material on the disc's surface.

## 3. RESULTS AND DISCUSSION

After completing the tests as per Taguchi $L_{16}$ array, the data taken from the data acquisition system is processed further in the form of specific wear rate and coefficient of friction values tabulated in Table 5. The coefficient of friction data is directly taken from the tribometer software. At the same time, the specific wear rate is cal–culated using Eq. (1), which shows the relationship bet–ween wear volume, applied load, and sliding distance [8].

$$\text{Specific wear rate, } k = \frac{V}{F * d}\,\mu m^3 \big/ Nm \qquad (1)$$

where,

$V$ = Wear volume, $\mu m^3$
$F$ = Applied load, N
$d$ = Sliding distance, m

### 3.1 Taguchi design analysis for the wear behavior

The signal-to-noise (S/N) ratio, proposed by Genichi Taguchi [23], is the ratio of mean to standard deviation where the mean represents the desired data while

standard deviation is the undesired data in the output response data. Taguchi has categorized the S/N ratio responses into three categories as 'smaller the better' (Eq. 2), 'nominal the better' (Eq. 3), and 'larger the better' (Eq.4) category.

$$\text{Smaller the better} = -10\log\Sigma\left(Y^2\right)/n \quad (2)$$

$$\text{Nominal the better} = 10\log\Sigma\left(\left(Y^2\right)/\sigma^2\right) \quad (3)$$

$$\text{Larger the better} = -10\log\Sigma\left(\left(1/Y^2\right)/n\right) \quad (4)$$

where,

- $Y$ Observed value for the specified factor level combination
- $n$ Number of responses in the factor level combination.
- $\sigma$ Standard deviation of the responses for all noise factors for the specified factor level combination.

For better service life of the components undergoing wear (such as automotive brake discs), the '*k*' value should be minimum. Therefore, the '*k*' should be considered in the 'smaller the better category.' Similarly, the '$\mu$' values should be high in braking/gripping applications and should be considered in the 'larger the better category.' In the present study, based on categorization, using Eq. (2) and Eq. (4), the S/N ratio is determined using Minitab statistical software and tabulated in Table 5 for comparison with the results obtained by the experiment.

**Table 5. Wear test parameters and results**

| Test No. | Parameters | | | Experimental results | | S/N ratio of results | |
|---|---|---|---|---|---|---|---|
| | F (N) | v (m/s) | T (°C) | $k$ ($\mu$m$^3$/Nm) | $\mu$ | $k$ (dB) | $\mu$ (dB) |
| 1 | 20 | 1.1 | 30 | 683.75 | 0.4514 | -56.698 | -6.9088 |
| 2 | 20 | 2.2 | 60 | 984.99 | 0.4473 | -59.869 | -6.988 |
| 3 | 20 | 4.4 | 120 | 1712.52 | 0.4394 | -64.673 | -7.1428 |
| 4 | 20 | 8.8 | 240 | 2654.98 | 0.4344 | -68.481 | -7.2422 |
| 5 | 40 | 1.1 | 60 | 804.37 | 0.4393 | -58.109 | -7.1448 |
| 6 | 40 | 2.2 | 30 | 995.62 | 0.4558 | -59.962 | -6.8245 |
| 7 | 40 | 4.4 | 240 | 2123.11 | 0.4358 | -66.54 | -7.2143 |
| 8 | 40 | 8.8 | 120 | 2565.61 | 0.4251 | -68.184 | -7.4302 |
| 9 | 80 | 1.1 | 120 | 1090.31 | 0.4303 | -60.751 | -7.3246 |
| 10 | 80 | 2.2 | 240 | 1648.74 | 0.4293 | -64.343 | -7.345 |
| 11 | 80 | 4.4 | 30 | 1514.68 | 0.446 | -63.606 | -7.0133 |
| 12 | 80 | 8.8 | 60 | 2135.93 | 0.4326 | -66.592 | -7.2783 |
| 13 | 160 | 1.1 | 240 | 1661.56 | 0.4074 | -64.41 | -7.7996 |
| 14 | 160 | 2.2 | 120 | 1627.42 | 0.4102 | -64.23 | -7.74 |
| 15 | 160 | 4.4 | 60 | 1769.99 | 0.4193 | -64.959 | -7.55 |
| 16 | 160 | 8.8 | 30 | 2174.21 | 0.416 | -66.746 | -7.6181 |

On observing the experimental results given in Table 5, it is found that test no. '1' reports the least value of *'k'* while test no. 6 reports the highest '$\mu$'value.

### 3.2 Effect of wear parameters on wear behavior (*'k', 'μ'*)

The effect of load, sliding velocity, and temperature over '*k*' (mean of means) is shown in Figure 3. It is observed that the '*k*' value increases initially with the rise in load value from 20 N to 40 N and remains almost constant between 40N to 80N load. The *'k'* value of the material increases again with an increase in load from 80 N to 160 N.

The '*k*' also increases with the sliding velocity and temperature increase. In the initial stage, It is observed that as the load is applied, the surface contact area between the pin and the disc is significantly less due to the contact between surface peaks on both disc and pin faces.

As the test progresses, the surface peaks are worn off and converted into wear debris, increasing the contact surface area. The '*k*' remains almost constant when the load varies from 40 N to 80 N. This '*k*' value may be attributed to wear debris that revolves around the disc surface under the pin contact region. At initial sliding velocity, the rubbing surfaces of the pin and disc are fine enough and start deteriorating with time with the increase in the sliding friction due to load and temperature. This increase in sliding friction results in the thermal softening of the surface material of the disc, which further helps kick off the surface molecules from the disc surface and results in surface wear. Such molecules get pile-ups to form lumps of wear debris. These wear lumps ran over and along the disc surface in the pin contact area and further helped enhance the surface wear rate by increasing the separation rate of more molecules from the disc surface and the pin surface. These debris lumps with sufficient mass intermittently runoff from the disc surface due to centrifugal forces. The minimum value of '*k*' is observed at 20 N load (sliding velocity of 1.1 m/s) and highest at 160 N (sliding velocity of 8.8 m/s) at room temperature. In contrast, at 240°C, the least '*k*' is found at 80 N (2.2 m/s) and 20 N (8.8 m/s) due to variation in the sliding friction.

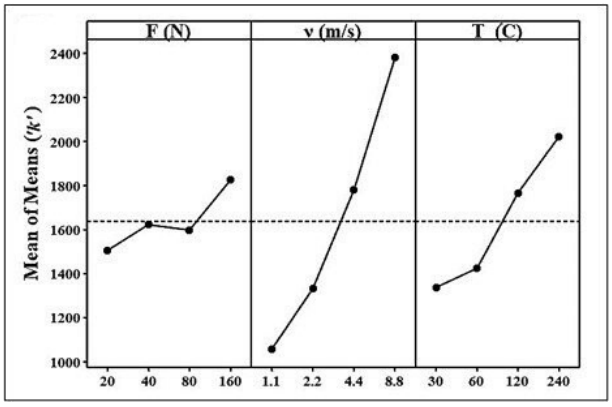


**Figure 3. Effect of wear parameters on *'k'***

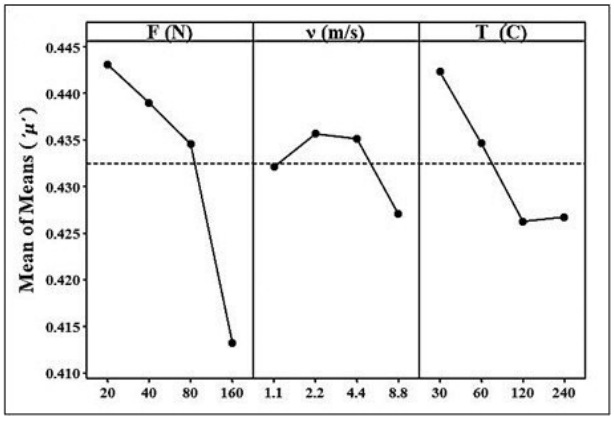


**Figure 4. Effect of wear parameters on *'μ'***

Figure 3 shows that the value of '*k*' increases with the increase in applied load, sliding velocity, and tempe–rature. A combination of 20 N load 1.1 m/s sliding velocity at room temperature 30°C results in the least '*k*', and the maximum wear is observed with extreme load, sliding velocity, and disc temperature values. The maxi–mum temperature reaches approxi–mately 190°C in an automotive disc brake with intermittent brake loads [25].

A higher *'μ'* is desired in braking applications. This study aims to optimize the *'μ'* of Si-Mo-Cr DCI for automotive brake disc applications. Figure 4 shows the effect of applied load, sliding velocity, and temperature on *'μ*.' On observing the effects of applied load, it is found that the value of *'μ'* is higher at lower loads, and as the load increase, it decreases slightly. Initially, at lower values of wear parameters, only the surface peaks are in contact during the rubbing action of the pin over the disc surface. This contact of peaks only resulted in higher values of *'μ'* and converted into wear debris due to the rubbing action of the pin over the disc surface. The formed wear debris remains in the pin-disc contact area. It revolves over the disc surface under the pin resulting in a slight decrease in *the 'μ'* value, which is visible when sliding velocity increases from 2.2 m/s to 4.4 m/s. The varying trend in *'μ'* values with an increase in sliding velocity is also depicted in Figure 4. The variation in obtained data may be attributed to the variation in sliding friction, debris lumps, and temperature. It is observed that *'μ'*initially increases with an increase in sliding velocity and then remains almost constant for sliding velocity ranging from 2.2m/s to 4.4m/s. After this, the *'μ'* value decreases with the increase in the sliding velocity. This decrease in friction value may be attributed to the stick and slip phenomenon of the rubbing surfaces. The *'μ'* value decreases as the temperature rises to 120°C and, after that, increases a little bit and almost remains constant. It indicates that the effect of temperature ceases to affect the value of *'μ'* and could be attributed to the thermal softening of the contacting surfaces. The highest value of *'μ'* is observed at 2.2 m/s, 20 N load, and room temperature conditions, while the least *'μ*' value is found at 8.8 m/s, 160 N load, and 120°C temperature.

### 3.3 Selection of optimum wear behavior conditions for '*k*' and *'μ'*

The S/N ratio response table obtained using Minitab software for '*k*' and *'μ'*are given in Table 6, and the va–riation are also shown in Figures 5 and 6, respectively.

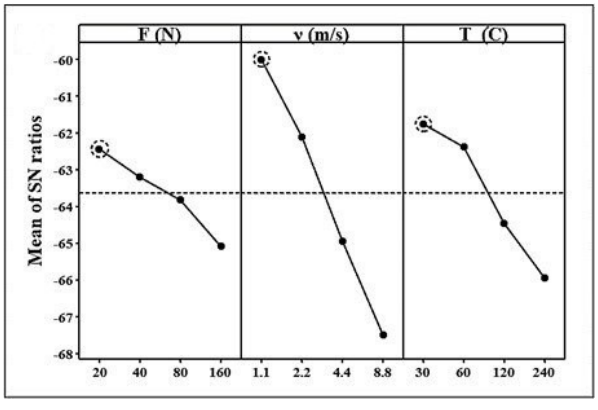


**Figure 5. Mean S/N ratio for optimum *'k'***

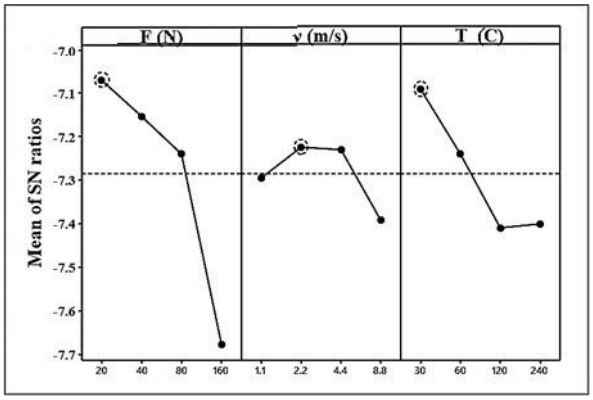


**Figure 6. Mean S/N ratio for optimum 'μ'**

A higher value of the S/N ratio depicts the minimum variation between the desired output and the measured output. The highest mean S/N ratio for '*k*', as shown in Figure 5, is observed at 20 N load, 1.1 m/s sliding velocity, and 30°C room temperature. Therefore, the predicted optimum process parameters for the least specific wear rate '*k*' are observed at an applied load of 20 N, 1.1 m/s of sliding velocity, and 30°C. The corresponding level values are highlighted in Table 6 and are represented as $F_1$-$v_1$-$T_1$ for the least '*k*' value in Figure 5. Also, the highest mean S/N ratio for *'μ'*in Figure 6 is observed at 20 N of applied load, 2.2 m/s sliding velocity, and 30°C, which differ from the experimental results obtained experimentally in test '6' of Table 5. Therefore, the predicted optimum process parameters for the highest value of the coefficient of friction *'μ'* using the Taguchi method are 20 N load, 2.2 m/s sliding velocity, and 30°C. The corresponding level values are highlighted in Table 6 and are represented as$F_1$-$v_2$-$T_1$ for the highest value of *'μ'* in Figure 6.

**Table 6.Mean S/N ratio response for '*k*' and *'μ'***

| S/N response | Wear parameters | Mean S/N ratio | | | | Delta | Rank |
|---|---|---|---|---|---|---|---|
| | | Level 1 | Level 2 | Level 3 | Level 4 | | |
| *k* | F (N) | **-62.43** | -63.2 | -63.82 | -65.09 | 2.66 | 3 |
| | v (m/s) | **-59.99** | -62.1 | -64.94 | -67.5 | 7.51 | 1 |
| | T ( □C) | **-61.75** | -62.38 | -64.46 | -65.94 | 4.19 | 2 |
| *μ* | F (N) | **-7.07** | -7.153 | -7.24 | -7.677 | 0.606 | 1 |
| | v (m/s) | -7.294 | **-7.224** | -7.23 | -7.392 | 0.168 | 3 |
| | T (□C) | **-7.091** | -7.24 | -7.409 | -7.4 | 0.318 | 2 |

### 3.4 Confirmation test

Confirmation tests are performed per the predicted optimal conditions for validating Taguchi's predicted optimum conditions. For estimating and verifying the responses at predicted optimum values, the predicted S/N ratio (ε) is used and calculated by using Eq. (5)[19].

$$\varepsilon_{predicted} = \varepsilon_l + \sum_{i=1}^{x}\left(\varepsilon_0 - \varepsilon_l\right) \quad (5)$$

where,

$\varepsilon_l$ Total mean S/N ratio

$\varepsilon_0$ Mean S/N ratio at an optimum level

$x$ No of input process parameters

In the present study, based on the S/N ratio response given in Table 6, it is found that the optimum level

parameters ($F_1$-$v_1$-$T_1$) for '*k*' matched with the wear parameters combination already selected and performed in test-1 ($F_1$-$v_1$-$T_1$) in Table 5. Based on this result, there is no need to repeat the experiment to find the least value of '*k*' for the selected wear parameters. Similarly, as per Table 6, the optimum level parameters for the highest value of *'μ'* are found as$F_1$-$v_2$-$T_1$, which does not match with any combination of wear parameters available in Table 5, and the confirmation test is performed for the same by using these optimal wear parameters highlighted in Table 6. The results for optimum values of '*k*' and *'μ'* are given in Table 7, respectively. The initial process parameters are chosen as $F_1$-$v_1$-$T_1$.

Table 7 shows similar values for optimum '*k*' and *'μ'* as selected as initial process parameters. No reduction is observed in the specific wear rate at optimum process parameters. Similarly, no change is found in the 'μ' value at optimal process para–meters. From the results, it is opined that the Taguchi optimization method signi–ficantly optimized the '*k*' and *'μ'* values for the wear behavior analysis of the specimens of Si-Mo-Cr DCI.

**Table 7. Mean S/N ratio response of specific wear rate '*k*' and coefficient of friction *'μ'***

| Particulars | Initial wear parameters | | Optimal wear parameters | | | |
|---|---|---|---|---|---|---|
| | | | Prediction | | Experiment | |
| | *k* | *μ* | *k* | *μ* | *k* | *μ* |
| Level | $F_1$- $v_1$-$T_1$ | $F_1$- $v_1$-$T_1$ | $F_1$- $v_1$-$T_1$ | $F_1$- $v_2$-$T_1$ | $F_1$- $v_1$-$T_1$ | $F_1$–$v_2$–$T_1$ |
| S/N ratio (dB) | -56.698 | -6.9088 | -56.906 | -6.8155 | -56.698 | -6.9088 |
| Results | 683.75 | 0.4514 | | | 683.75 | 0.4514 |

### 3.5 ANOVA for *'k'* and *'μ'*

The performance-affecting parameters are obtained by ANOVA analysis. The ANOVA results for *'k'* and *'μ'* are given in Table 8. From Table 8, it is noticed that *'k'* is significantly influenced by the sliding velocity (68.41%) followed by temperature (23.57 %) and load (8.02 %), respectively. Similarly, it is found that *'μ'* is significantly influenced by load (71.65 %) followed by temperature (22.35 %) and sliding velocity (6 %), respectively. The temperature has balanced effects on both 'k' and 'μ' values. From ANOVA analysis, it is perceived that load has the least influence on '*k*' and is highest on *'μ'* values, while sliding velocity has the least influence on *'μ'* and is highest on '*k*' values.

**Table 8. ANOVA response for *'k'* and *'μ'***

| Source | Degree of freedom | Specific wear rate, k | | | Coefficient of friction μ | | |
|---|---|---|---|---|---|---|---|
| | | Sum of squares | Mean squares | % Share | Sum of squares | Mean squares | % Share |
| F (N) | 3 | 15.137 | 5.0456 | 8.02 | 0.8755 | 0.2918 | 71.65 |
| v (m/s) | 3 | 129.131 | 43.0437 | 68.41 | 0.0732 | 0.0244 | 6 |
| (°C) | 3 | 44.48 | 14.8267 | 23.57 | 0.2733 | 0.0911 | 22.35 |
| Total | 9 | 188.748 | | 100 | 1.222 | | 100 |

### 3.6 Modeling for *'k'* and *'μ'*

In the present study, predictive mathematical models for the dependent variable parameters of *'k'* and *'μ'* as a function of applied load, sliding velocity, and tempe–rature, using the linear regression analysis in Minitab software, have been developed. The prophetic equations obtained from the first-order linear regression analysis for *'k'* and *'μ'* are given in Eq. 6 and 7, respectively.

$$k = 421.0 + (1.906 * F) + (169.38 * \nu) + (3.303 * T) \quad \left(\mathbf{R}^2 = 97.05\%\right) \tag{6}$$

$$\mu = 0.4593 - (0.00022 * F) + (0.0086 * \nu) - (0.00007 * T) \quad \left(\mathbf{R}^2 = 85.84\%\right) \tag{7}$$

The potentiality of the developed models for *'k'* and *'μ'* is checked by the correlation coefficient '$R^2$' [26]. The value of '$R^2$' varies from zero to one, and the values closer to one indicate a good fit for the developed regression model. In the present study, the value of '$R^2$' for *'k'* and *'μ'* is founded as 97.05% and 85.84%, res–pectively. The normal probability plots for *'k'* and *'μ'* residuals are shown in Figures 7 and 8, respectively. The closeness to the straight line of the residual plot in–dicates the normal distribution of the residual error and correlation coefficient significance. These residual plots are also validating the developed regression models.

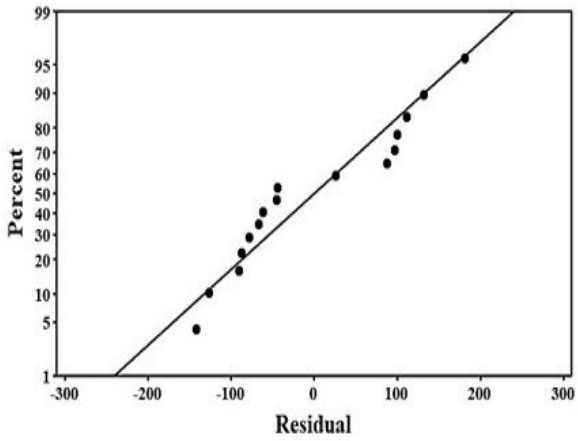


**Figure 7. Normal probability plot of the residual of *'k'***

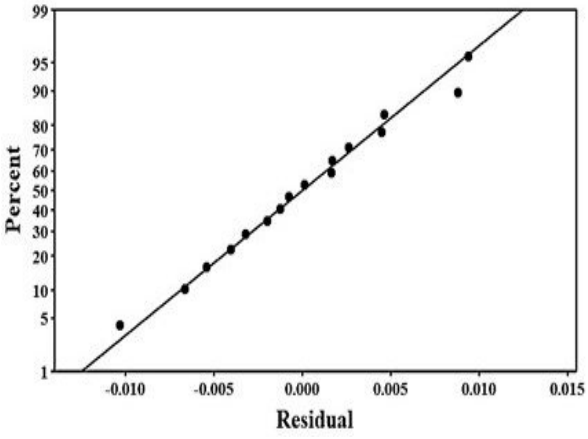


**Figure 8. Normal probability plot for the residual of *'μ'***

The confirmation tests are conducted for the ran–domly chosen wear test data given in Table 5, and the comparison of experimental and predicted results is

tabulated in Table 9. Table 9 shows that the predicted and experimental results are in good agreement. It is opined that the percentage error using Eq. 6 and 7, respectively, varies from 2.68 % to 7.07% for 'k' values while 0.21% to 5.95% for 'μ' values.

**Table 9. Confirmation results for the developed models**

| Test no. | Experimental results | | Predicted results | | Residual | | % Error | |
|---|---|---|---|---|---|---|---|---|
| | *k* | *μ* | *k* | *μ* | *k* | *μ* | *k* | *μ* |
| 2 | 984.995 | 0.447 | 1029.9 | 0.453 | -44.941 | -0.0057 | 4.56 | 1.27 |
| 4 | 2654.98 | 0.434 | 2742.4 | 0.4468 | -87.399 | -0.0124 | 3.29 | 2.85 |
| 6 | 995.619 | 0.456 | 968.97 | 0.4507 | 26.6533 | 0.00506 | 2.68 | 1.12 |
| 8 | 2565.61 | 0.425 | 2384.1 | 0.4504 | 181.465 | -0.0253 | 7.07 | 5.95 |
| 10 | 1648.74 | 0.429 | 1738.8 | 0.4284 | -90.095 | 0.0009 | 5.46 | 0.21 |
| 12 | 2135.93 | 0.433 | 2262.2 | 0.4459 | -126.28 | -0.0133 | 5.91 | 3.07 |
| 14 | 1627.42 | 0.41 | 1495 | 0.4194 | 132.468 | -0.0092 | 8.14 | 2.24 |
| 16 | 2174.21 | 0.416 | 2315.6 | 0.4309 | -141.39 | -0.0149 | 6.5 | 3.58 |

The contour plots in Figure 9 show the relationship among the wear parameters concerning specific wear rate and coefficient of friction. Figure(a, b, c) shows the color scheme, in the form of inclined strips, lighter to dark from initial to final values of wear parameters for specific wear rate. While Figure 9 (d, e, f) shows the color scheme, in the form of inclined color strips, darker to light, to show the variation in coefficient of friction values in respect of wear parameters. These contour plots are very useful in accessing the response parameters for the different com–binations of wear parameters.

On examining Figure 9(a), it is observed that the lower value of '*k*' (< 1200 μm$^3$ /Nm) obtained within the triangular area represented by the lightest color shade comprising of the applied load (up to 100 N) and sliding velocity (up to 2 m/s) only. While within the triangular area representing the darkest color shade comprising of an applied load value up to 50 N and sliding velocities up to 8 m/s, the higher value of '*μ'* (> 0.44) is obtained, as shown in Figure 9 (d).

Also, on examining Figure9(b, e), the plots between applied load and temperature, the lower value of '*k*' (< 1400 μm$^3$/Nm) obtained within the triangular area repre–sents the lightest color comprising the applied load (up to 70 N) and up to 60°C temperature only. While within the triangular area representing the darker color comprising of applied load value (up to 65 N) and up to 170 °C tempe–rature shows the higher value of '*μ'* (>0.44), respectively. 1200 μm$^3$/Nm) obtained within the triangular area repre–sents the lightest color comprising the sliding velocities (up to 2.2m/s) and up to 70 °C temperature only. While within the triangular area comprising the darker color among sliding velocities value (up to 5m/s) and up to 80 °C.

Similarly, on examining Figure 9 (c,f), the plots bet–ween sliding velocity and temperature, the lower value of '*k*' (<1000 μm$^3$/Nm) obtained within the triangular area represents the lightest color comprising the sliding velocities (up to 2.2m/s) and up to 70°C temperature only. While within the triangular area comprising the darker color among sliding velocities value (up to 5m/s) and up to 80°C temperature shows the higher value of *'μ'* (> 0.436) respectively. From Figure 9, the values of 'k' and 'μ' may be estimated significantly at different load, sliding velocity, and temperature combinations.

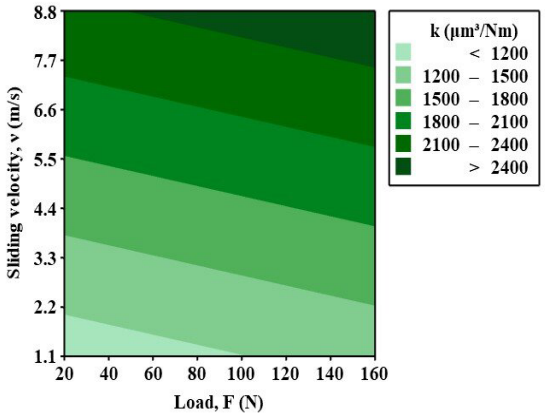


**Specific wear rate vs. sliding velocity and load**

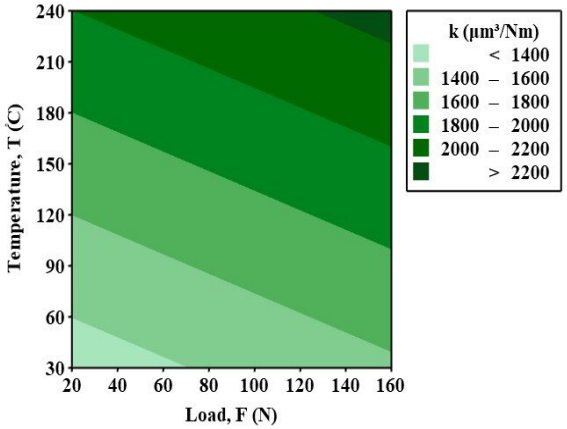


**Specific wear rate vs. temperature and load**

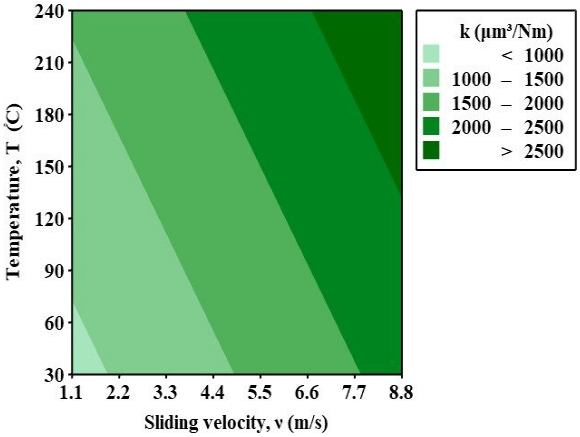


**Specific wear rate vs. sliding velocity and load**

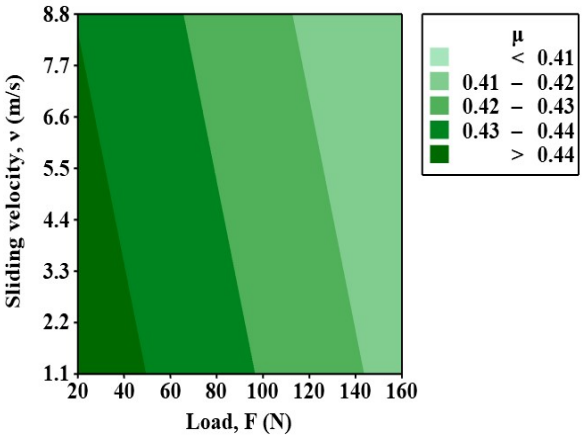


**Coefficient of friction vs. sliding velocity and load**

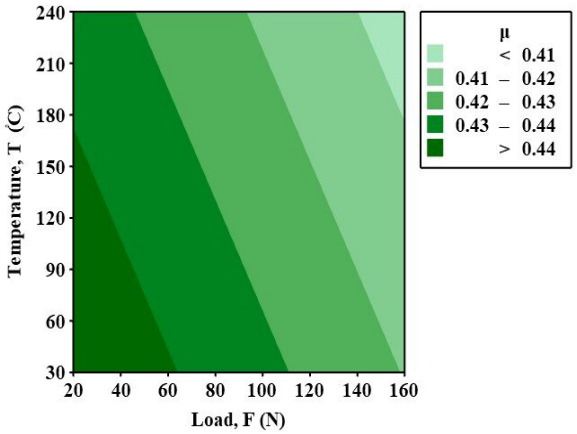


**(e) Coefficient of friction vs. temperature and load**

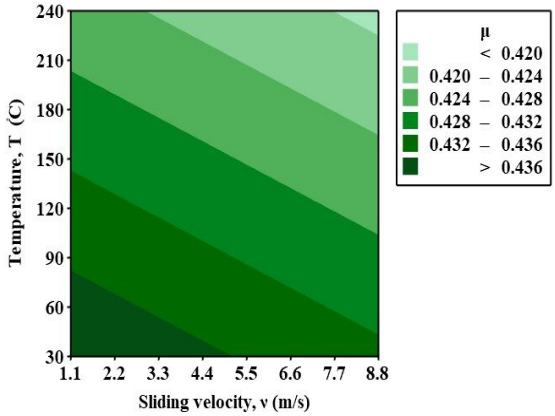


**(f) Coefficient of friction vs. sliding velocity and load**

**Figure 9.Contour plots of specific wear rate and coefficient of friction vs. load, sliding velocity, and temperature**

### 3.7 SEM and EdX analysis

The representative images of the disc's wear surface, obtained from the scanning electron microscope, are shown in Figure 10, in which two different micrographs of the wear surface of the discs are shown. From Figure 10(a, b), it is observed that the wear debris formed during the sliding of the disc under the loaded pin at a controlled temperature gets lodged onto the surface of the disc, forming a wear lump which further helps in accelerating the wear rate of the disc surface. Some wear lumps intermittently move out of the surface contact area between the pin and disc under the influence of centrifugal action.

In observing Figure 10 (a), the wear track traces are visible on the disc surface. The friction material of the pin is also found embedded on the surface. As the friction material is non-conducting in nature, the shadow of the friction material particles is also clearly visible. In Figure 10 (b), the chipping-off of the material from the disc surface is visible. μm

Figures 11 and 12 show the energy dispersive x-ray microanalysis of the representative wear surface. The per–centage of the embedded microconstituents in the tabular form is in Table 10. Figure 12 and Table 10 show that some wear debris is significantly embedded over the disc's surface. These embedded wear debris, having iron as a significant contributor, comprise the few alloying elements of both disc surface and pin material. However, no Ti, V, or Sb traces are found embedded over the disc surface.

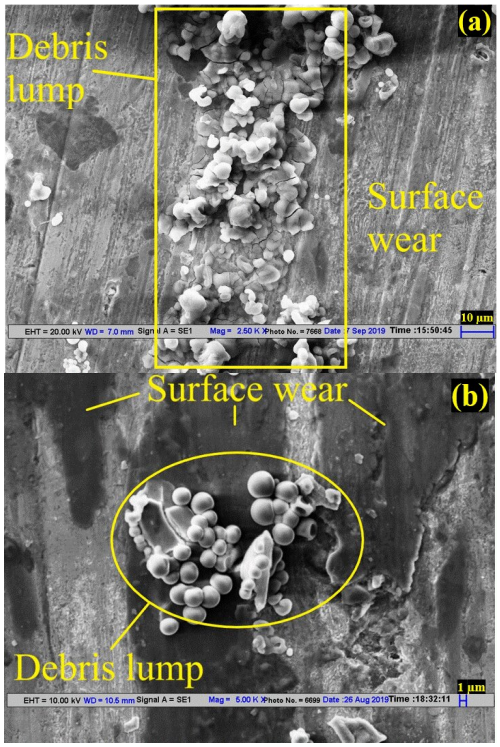


**Figure 10. Micrographs of the wear surface of the representative disc**

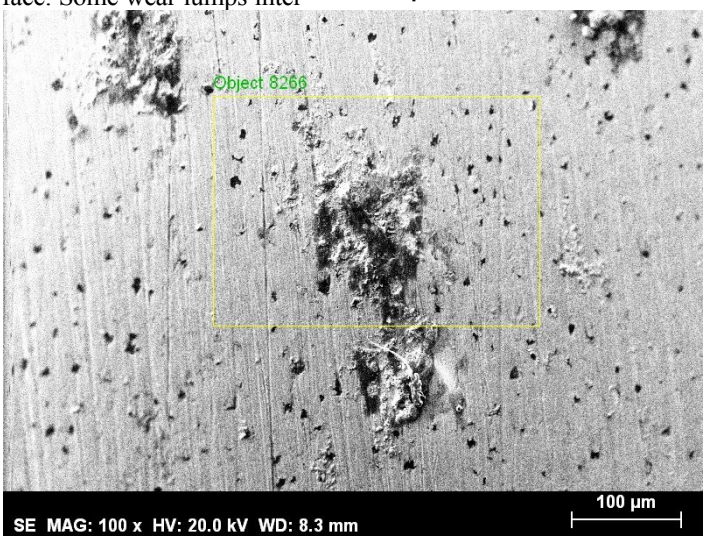


**Figure 11. Micrographs of wear surface**

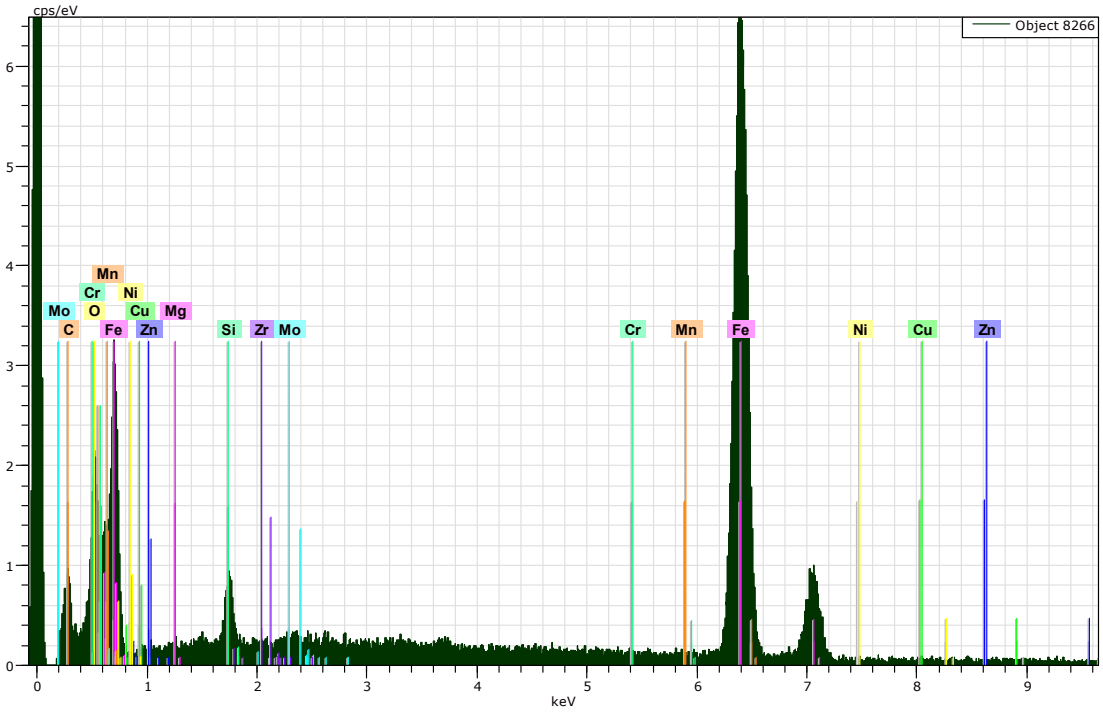


**Figure 12. EdX plot of representative wear surface of the disc**

**Table 10. composition of embedded material on the wear surface of the representative disc**

| Element | Fe | O | Mg | Si | C | Cu | Mo | Ca | Ni | Mn | Cr | Zr |
|---|---|---|---|---|---|---|---|---|---|---|---|---|
| (%wt.) | 71 | 12 | 4.5 | 3.7 | 2.7 | 1.5 | 1.5 | 1.1 | 0.8 | 0.7 | 0.4 | 0.3 |

## 4. CONCLUSIONS

The dry sliding wear properties, viz., specific wear rate and coefficient of friction of the specimens of Si-Mo-Cr ductile cast iron against the brake pad friction material, are studied using a series of pin-on-disc experiments. Four wear parameters are selected for studying the behavior of the disc surface against a pin made from brake pad material. Taguchi $L_{16}$ array is used for optimizing the sliding wear parameters. The discs are made from the as-cast Si-Mo-Cr ductile cast iron, and the pins are fabricated from brake pad materials extensively used in automotive. After conducting the pin-on-disc tests as per Taguchi $L_{16}$ array, the results are further processed and modeled using analysis of variance and first-order regression analysis. Confirmation tests were also done, and observed that the experimental results were in close agreement with the predicted results obtained using first-order regression equations. From the results, it is concluded that:

- The sliding velocity significantly influences the specific wear rate, whereas the applied load is the key influencing parameter for a higher friction coefficient value. The temperature is an optimum influencer on both sliding wear rate and coefficient of friction.
- Unambiguously, the minimum value of *'k'* and the higher value of *'μ'* is obtained at the lower level of the preselected wear parameters.
- SEM and EdX analysis of disc wear surfaces show that the wear debris embedded in the disc surface is at higher wear parameters.
- From confirmation tests based on first-order regression analysis, it is also found that the experimental results are in good agreement with the predicted results. The experimental values of *'k'* and *'μ'* at the rest of the preselected wear parameters are very close to the predicted data values using first-order regression analysis.
- Contour plots reveal that the minimum *'k'* value may be obtained within the triangular region lighter in color. Any combination of the wear parameters within the region may result in a minimum *'k'* value of disc material.
- Similarly, the maximum *'μ'* value may be obtained within the triangular region darkest in color in contour plots drawn to maximize this value. Any combination of wear parameters may result in a higher *'μ'* value.


## ACKNOWLEDGMENT

We are very thankful to the Department of Mechanical Engineering, Delhi Technological University, for providing the requisite facilities to carry out this research. We sincerely thank anonymous referees for their valuable suggestions. No separate funding is received for this research.


## REFERENCES:


[1] Shafiee A., Nili-Ahmadabadi M., Ghasemi H.M. Hossein-Mirzaei E.: Wear behaviour of a Cr-Mo steel with different microstructures, in comparison with austempered ductile iron (ADI), Int J Material Forming, Vol. 2, No.1 pp. 237-241,2009. https://doi.org/10.1007/s12289-009-0636-0

[2] Aal A.A., Ibrahim K.M., Hamid ZA.: Enhancement of wear resistance of ductile cast iron by Ni–SiC composite coating, Wear, Vol. 260, No.9-10, pp. 1070-1075,2006. https://doi.org/10.1016/j.wear.2005.07.022

[3] Delprete C., Sesana R.: Experimental characterization of a Si – Mo – Cr ductile cast iron, Jmaterials & Design, Vol. *57*, pp. 528–537, 2014. https://doi.org/10.1016/j.matdes.2014.01.002

[4] Abedi H.R., Fareghi A., Saghafian H., Kheirandish S.H.: Sliding wear behavior of a ferritic–pearlitic ductile cast iron with different nodule count, Wear, Vol. 268, No. 3-4, pp. 622-628,2010. https://doi.org/10.1016/j.wear.2009.10.010

[5] Babazadeh M., PourAsiabi H. PourAsiabi H.: Wear characteristics of ADIs: a comprehensive review on mechanisms and effective parameters, J. Basic. Appl. Sci. Res., Vol.3, No.2, pp.646-656, 2013.

[6] Fontanari V., Benedetti M., Girardi C., Giordanino L.: Investigation of the lubricated wear behavior of ductile cast iron and quenched and tempered alloy steel for possible use in worm gearing, Wear, Vol. 350, pp. 68-73,2016. https://doi.org/10.1016 /j.wear.2017.02.029

[7] Zhang D., Li Y., Du X., Fan H., Gao F.: Microstructure and tribological performance of boride layers on ductile cast iron under dry sliding conditions, Engineering Failure Analysis, Vol. 134, 106080, 2022. ttps://doi.org/10.1016/j.engfailanal.2022.106080

[8] Stachowiak GW and Batchelor AW.:*Engineering tribology*, Butterworth-heinemann, 2013.

[9] Basurto-Hurtado J.A., Morales-Hernández L.A., Osornio-Rios R.A., Dominguez-Gonzalez A.: An Approach Based on the Exploratory Data Analysis to Relate the Wear Behavior with the Microstructure of Ductile Cast Irons, Advances in Materials Science and Engineering, Vol.2016, Article ID 2605602, pages 11,2016. https://doi.org/10.1155/2016/2605602

[10] Mardaras E., González-Martínez R., Bayon R., Nastac L. and Méndez S.: Surface modification of ductile iron produced by an innovative in-situ casting technique, International Journal of Cast MetalsResearch, Vol. 33, pp. 103-111,2020.

https://doi.org/10.1080/13640461.2020.1766278

[11] Cardoso P.H.S., Israel C.L. Strohaecker T.R.: Abrasive wear in Austempered Ductile Irons: A comparison with white cast irons. Wear, Vol. 313, 29-33,2014.https://doi.org/10.1016/j.wear.2014.2.009

[12] Zou J. P., Shimizu K., Cai Q.Z.: Effects of Cr Content and Annealing Temperature on Microstructure and Wear Characteristics of Cast Ausferrite Nodular Iron, Journal of Iron and Steel Research, International, Vol. 22, No.11, pp. 1049-1054,2015.https://doi.org/10.1016/S1006-706X(15)30111-4

[13] Rebasa N., Dommarco R. and Sikora J.: Wear resistance of high nodule count ductile iron, Wear, Vol. 253, pp. 855-861,2002. https://doi.org/10.1016/S0043-1648(02)00171-0

[14] Weiß P., Tekavčič A., Bührig-Polaczek A.: Mechanistic approach to new design concepts for high silicon ductile iron, Materials Science and Engineering: A, Vol. 713, pp. 67-74,2018. https://doi.org/10.1016/j.msea.2017.12.012

[15] Scandian C., Boher C., De Mello J. D. B., Rezai-Aria F.: Effect of molybdenum and chromium contents in sliding wear of high-chromium white cast iron: The relationship between microstructure and wear, Wear, Vol. 267*,* No.1-4, pp. 401-408, 2009.

[16] Selvaraj T., Hariharasakthisudhan P., Pandiaraj S., Sathickbasha K., Aslam N. M. A.: Optimizing the design parameters of radial tip centrifugal blower for dust test chamber application through numerical and statistical analysis. FME Transactions, Vol.*48,* No.1, pp. 236-245, 2020.

[17]Prasad B.: Sliding wear response of a cast iron under varying test environments and traversal speed and pressure conditions, Wear, Vol. 260, pp. 1333-1341,2006. https://doi.org/10.1016/j.wear.2005.09.017

[18] Prasad B.: Sliding wear response of a grey cast iron: Effects of some experimental parameters, Tribology International, Vol. 44, pp. 660-667,2011. https://doi.org/10.1016/j.triboint.2011.01.006

[19] Sahin Y. and Durak O.: Abrasive wear behaviour of austempered ductile iron, Materials & Design, Vol. 28, pp. 1844-1850,2007. https://doi.org/10.1016/j.matdes.2006.04.015

[20] Kuti, R., Könczöl, F., Csapó, L., Földi, L., Tóth, Á. D. (2022). Detection of the possible engine damages in case of a continuous track military vehicles with tribological investigations. FME Transactions, 50(3), pp. 526-534

[21]Kshirsagar M. P., and Khairnar H.: Investigation of coefficient of friction at the interface of automobile brake pads using Greenwood-Williamson contact model and novel test rig. FME Transactions, Vol. 50, No.3, pp 561-575, 2020.

[22] Chernets M., Kornienko A., ChernetsY., Fedorchuk, S.: Analytical assessment of the sliding friction coefficient influence on durability, wear and contact pressure in spur gears. FME Transactions, Vol. 49, No.2, 472-479, 2021.

[23]Taguchi G.: System of experimental design; engineering methods to optimize quality and minimize costs. 1987.

[24]Ram N., Gautam V.: Evaluation of Johnson-Cook material model parameters for Si-Mo-Cr ductile cast iron. Materials Today Proceedings, Vol. *61*, pp. 16-20, 2022. https://doi.org/10.1016/j.matpr.2022.03.298

[25] Talati F. and Jalalifar S.: Analysis of heat conduction in a disk brake system. Heat and mass transfer, Vol. 45, pp. 1047-1059, 2009. https://doi.org/10.1007/s00231-009-0476-y

[26] Montgomery D.C.:*Design and analysis of experiments*. John Wiley & sons, 2017.

**NOMENCLATURE**

| | |
|---|---|
| Si | Silicon |
| Mo | Molybdenum |
| Cr | Chromium |

| | |
|---|---|
| C | Carbon |
| Cu | Copper |
| Mg | Magnesium |
| Fe | Iron |
| $k$ | Specific wear rate |
| μ | Coefficient of friction |
| P | Phosphorus |
| S | Sulphur |
| Ti | Titanium |
| V | Vanedium |
| Mn | Manganese |
| Zn | Zinc |
| Zr | Zirconium |
| Sb | Antimony |
| Al | Aluminum |
| F | Applied load (N) |
| d | Sliding distance (m) |
| $V$ | Wear volume ($\mu m^3$) |
| Y | Response for the given factor level combination |
| n | Number of responses in the factor level combination |
| σ | Standard deviation of the responses for all noise factors for the given factor level combination. |
| $v$ | Sliding velocity (m/s) |
| $\varepsilon_l$ | Total mean S/N ratio |
| $\varepsilon_0$ | Mean S/N ratio at an optimum level |
| x | No of input process parameters |

**ACRONYMS**

| | |
|---|---|
| Si-Mo-Cr | Silicon-molybdenum-chromium |
| SEM | Scanning electron microscope |
| EdX | Energy dispersive X-ray |
| DCI | Ductile cast iron |

## КАРАКТЕРИЗАЦИЈА СУВОГ КЛИЗНОГ ПОНАШАЊА Si-Mo-Cr НОДУЛАРНОГ ЛИВЕНОГ ГВОЖЂА

**Н. Рам, В. Гаутам**

Предуслови за материјал кочионог диска укључују нижу специфичну стопу хабања, висок коефицијент трења о материјал кочионих плочица, мању тежину и већу стопу одвођења топлоте. Ово истраживање проучавало је понашање клизног хабања у сувом стању Si-Mo-Cr дуктилног ливеног гвожђа (ДЦИ). Серија тестова хабања пин-он-дисц се спроводи ко–ришћењем Тагучи L16 низа за оптималну комби–нацију оптерећења, брзине клизања и температуре на ротационом трибометру на контролисаним тем–пературама у распону од 30°C до 240°C. Анализа варијансе, регресиона анализа првог реда и тестови потврде се раде да би се потврдили резултати добијени за својства хабања материјала. Такође се ради СЕМ и ЕдКс анализа хабајућих површина. Утврђено је да брзина клизања има значајнији утицај на специфичну стопу хабања. Насупрот томе, примењено оптерећење је кључни параметар који утиче на већу вредност коефицијента трења.